arXiv:cond-mat/9910231v3 [cond-mat.str-el] 19 Aug 2003

cond-mat/9910231

Translational symmetry breaking in two-dimensional antiferromagnets and superconductors

Subir Sachdev and Matthias Vojta

Department of Physics, Yale University,
P.O. Box 208120, New Haven CT 06520-8120

(Dated: October 6, 1999)

Abstract

It was argued many years ago that translational symmetry breaking due to the appearance of spin-Peierls ordering (or bond-charge stripe order) is a fundamental property of the quantum paramagnetic states of a large class of square lattice antiferromagnets. Recently, such states were shown to be a convenient point of departure for studying translational symmetry breaking in doped antiferromagnets: these results are briefly reviewed here with an emphasis on experimental implications. In the presence of stronger frustration, it was also argued that the insulating antiferromagnet can undergo a transition to a deconfined state with no lattice symmetry breaking. This transition is described by a fully-frustrated Ising model in a transverse field: details of this earlier derivation of the Ising model are provided here—this is motivated by the reappearance of the same Ising model in a recent study of the competition between antiferromagnetism and d-wave superconductivity by Senthil and Fisher.

Proceedings of the International Workshop on **Magnetic Excitations in Strongly Correlated Electrons**, Hamamatsu, Japan, August 19-22, 1999. Journal of the Physical Society of Japan **69**, Supplement B, 1 (2000).

I. INTRODUCTION

Following the fundamental neutron scattering observations of Tranquada[1], there has been a vigorous resurgence[2, 3] in the study of states of two-dimensional strongly correlated systems which break various types of translational symmetries (to be precise: we will consider translational symmetry to be broken when an observable invariant under spin rotations (and which does not change the net charge of the system) does not remain invariant under the space-group of the lattice). In an early discussion of translational symmetry breaking in two-dimensional antiferromagnets[4, 5] it was argued that any quantum paramagnet accessed by a continuous quantum transition from a Néel state must have (for $S = 1/2$ spins) (i) broken translational symmetry due to spin-Peierls (or *bond*-charge density) ordering, and (ii) confinement of spin-1/2 excitations resulting in integer spin quasiparticle modes. Other early work[6, 7] used Hartree-Fock theory to study the formation of *site*-charge density order in lightly doped antiferromagnets. In this paper, we shall review recent work[8, 9] in which these two apparently divergent physical effects were studied in a combined footing—we shall argue that such an analysis leads to considerable physical insight and has significant experimental implications.

This paper is organized as follows. In Section II we will consider translational symmetry breaking in the quantum paramagnetic phases of insulating antiferromagnets—this will be done using lattice 'height' and Ising models which are obtained after a duality transformation. In Section III we will turn to the recent results[8, 9] on doped antiferromagnets, and their implication for experiments.

II. INSULATING ANTIFERROMAGNETS

A convenient and physically transparent framework for discussing the physics of the low-lying singlet excitations of a quantum paramagnet is the "quantum dimer model"[10]. At first glance, the formulation of the dimer model does appear rather arbitrary, with a number of ad hoc assumptions which obscure the connection to the Heisenberg antiferromagnet—instead, the dimer model is best viewed as a caricature which captures some essential pieces of the physics. We shall mainly use the dimer model as an intuitive intermediate step towards introducing dual 'height' and Ising models. These dual models have also been derived by a number of other methods, including systematic semiclassical and large N expansions[4, 5], and these provide the more formal justifications for the arguments here. We will describe duality transformations on an effective model of resonating singlet bonds which show that unfrustrated antiferromagnets are described by an effective height model in 2+1 dimensions[5, 12, 13]; in the presence of frustration, the height model gets modified to a fully frustrated, two-dimensional Ising model in a transverse field[14]. All of the results in this section were derived and published some time ago[5, 12, 13, 14] ; the frustrated Ising model was derived by one of us[15] and the main results were outlined in Ref.[14] , but details have not been previously published. The presentation of the details here was motivated by the reappearance of the same Ising model in a recent study of the competition between antiferromagnetism and d-wave superconductivity by Senthil and Fisher[16]. We also note another recent study of lattice gauge theory models of two-dimensional antiferromagnets by Nagaosa and Lee[17]; they examine theories related to those considered in Ref[13] and in the present paper, but their actions do not contain the crucial Berry phase terms (as in (2.16), (2.17), and (2.25)) associated with the non-zero net matter density on each site even in the

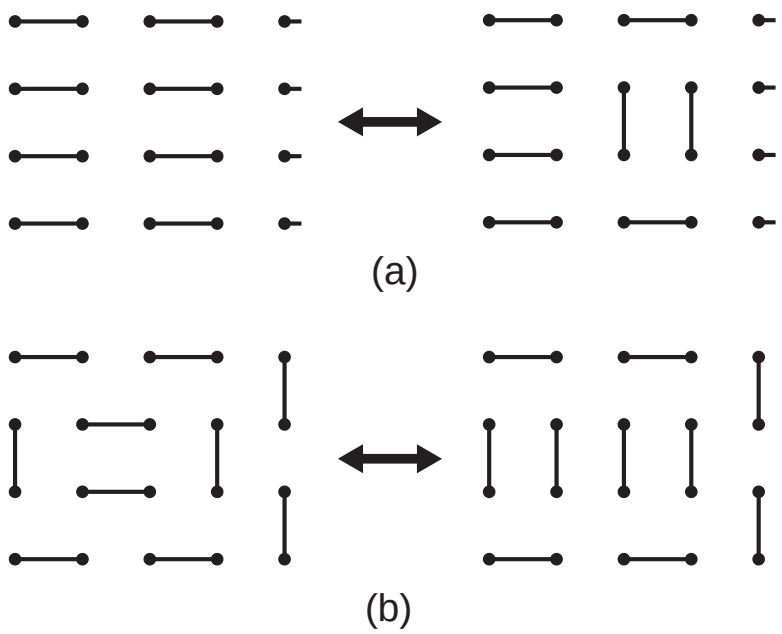

FIG. 1: Dimer coverings of the square lattice, each representing a distinct state in the singlet Hilbert space. The two states in (a) can resonate with each other as can the two in (b). The columnar state in (a) has the maximum number of resonating partners, and this drives the translational symmetry breaking.

undoped antiferromagnet—it is these Berry phase terms which are responsible for frustration in the dual height or Ising spin representation, and we believe their incorporation is essential for a proper description of the physics.

The central assertion of the dimer model is that it is appropriate identify the Hilbert space of the low-lying singlet excitations of the quantum paramagnet on a square lattice with a set of dimer coverings[10]. Each dimer covering corresponds to different singlet state, and off-diagonal matrix elements between such states therefore lead to a "resonance" between the dimers. Such resonance terms must preserve the constraint of one and exactly one dimer terminating at every site, and this severely restricts their form. Two possible resonating terms are illustrated in Fig 1. One might now anticipate that the ground state of such a resonating-valence-bond Hamiltonian is a liquid-like superposition of all dimer coverings, but this turns out not to be the case. The ground state in fact breaks lattice translational symmetry[4, 5] *e.g.* for some range of parameters it looks like the columnar ordered state at the top of Fig 1. There is a simple intuitive reason for this: the columnar state has the maximum number of plaquettes about which the dimers are able to resonate and still preserve the local constraints. This resonance lowers its energy, and this effect is strong enough that the system always picks out one of the four columnar states and retains memory of its orientation. The ordering is therefore due to a quantum "order-from-disorder" effect.

Let us now make these arguments more precise. We will divide our discussion into two subsections. Section II A will consider the model with dimers connecting nearest neighbors on the square lattice. More generally, the results here will apply to bipartite lattices in which the dimers only connect sites on opposite sublattices. We will show that such models here are described by effective height models in 2+1 dimensions[5, 13]. Section II B will consider

models in which the dimers are allowed to connect sites on the same sublattice—the effective model for these will be the fully frustrated Ising model in a transverse field[14].

A. Bipartite dimer models

We will only discuss the case of the nearest-neighbor, square lattice dimer model here. We identify the dimers by site, i, of the square lattice on their lower or left end. Let $\eta_i \hat{E}_{i\alpha}$ be the number operator for the dimer on site i oriented in the α direction ($\alpha = x, y$); η_i indicates the sublattice of site i, and equals $+1$ on one sublattice and -1 on the other. We have so far considered only a $S = 1/2$ antiferromagnet, but for general S there will be exactly $2S$ dimers emerging from every site—this constraint translates to

$$\Delta_\alpha \hat{E}_{i\alpha} = 2S\eta_i, \tag{2.1}$$

where Δ_α is the discrete lattice derivative in the α direction. The factors of η_i where introduced so that the constraint would have the Gauss-law form in (2.1), and the operator $\hat{E}_{i\alpha}$ is seen to be the analog of the electric field[12]. We also introduce an angular phase variable, $\hat{A}_{i\alpha}$ (the analog of a compact $U(1)$ gauge field), on every link which is canonically conjugate to $\hat{E}_{i\alpha}$:

$$[\hat{A}_{i\alpha}, \hat{E}_{j\beta}] = i\delta_{ij}\delta_{\alpha\beta}, \tag{2.2}$$

where it should be clear from the context when we mean $i = \sqrt{-1}$, and when i is a site label.

We can now write down the Hamiltonian of the dimer model:

$$H_d = \frac{K_1}{2} \sum_{i,\alpha} \hat{E}_{i\alpha}^2 - K_2 \sum_i \cos(\epsilon_{\alpha\beta}\Delta_\alpha \hat{A}_{i\beta}). \tag{2.3}$$

The first term, proportional to K_1 is only non-trivial when $2S > 1$, and it ensures that the density of dimers is as uniform as possible. It follows from the commutation relations (2.2) that the second term, proportional to K_2, flips dimers around a plaquette and so induces the 'resonance' shown in Fig 1.

We will now write down a path integral representation of the partition function of H_d by following a standard route. We insert complete sets of $\hat{E}_{i\alpha}$ eigenstates at small imaginary time intervals $\Delta\tau$. The matrix elements of the cosine term in H_d are evaluated by replacing it with the Villain periodic Gaussian form (this is the only 'approximation' made in our duality mappings - all other transformations below are exact):

$$\exp\left(K_2\Delta\tau\cos(\epsilon_{\alpha\beta}\Delta_\alpha\hat{A}_{i\beta})\right) \to \sum_{B_a} \exp\left(-\frac{B_a^2}{2K_2\Delta\tau} + iB_a\epsilon_{\alpha\beta}\Delta_\alpha\hat{A}_{i\beta}\right). \tag{2.4}$$

Here B_a is an integer-valued field on the sites, a, of the dual lattice; there is an obvious relationship between the location of the direct lattice site, i, and the dual lattice site a, but we will not specify it explicitly to avoid cluttering up the notation (we will consistently use the labels $i, j \ldots$ for sites on the direct lattice, and the labels $a, b \ldots$ for sites on the dual lattice). In the present case, a resides at the center of plaquette around which the 'flux' $\epsilon_{\alpha\beta}\Delta_\alpha\hat{A}_{i\beta}$ resonates the dimers. It is also convenient to introduce a three-vector notation in space time: we define the integer-valued 'electromagnetic flux' vector $F_{a\mu} = (E_{iy}, -E_{ix}, -B_a)$

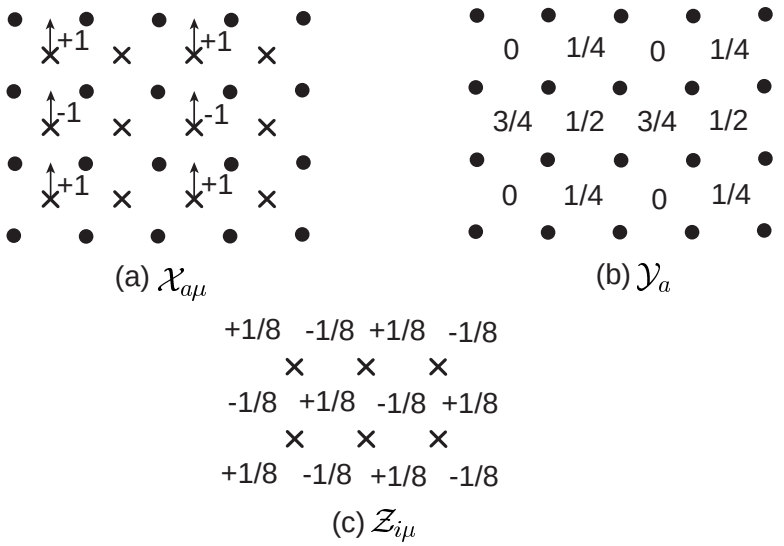

FIG. 2: The values of the only non-zero components of the fixed field $\mathcal{X}_{a\mu}$, $\mathcal{Y}_a$, and $\mathcal{Z}_{i\mu}$. The circles (crosses) are the sites of the direct (dual) lattice. In (c), only the $\mu = \tau$ component of $\mathcal{Z}_{i\mu}$ is non-zero and its values are shown.

on the dual lattice sites, where the index $\mu = (x, y, \tau)$ (we will consistently use the labels $\alpha, \beta \ldots$ to represent spatial components only, while $\mu, \nu, \lambda \ldots$ will represent three-dimensional spacetime components). Here $E_{i\alpha}$ refer to the integer eigenvalues of the operator $\hat{E}_{i\alpha}$ which are summed over in each time step. Now the partition function of H_d can be written in the compact form

$$Z_F = \sum_{\{F_{a\mu}\}} \exp\left(-\frac{e^2}{2}\sum_{a,\mu} F_{a\mu}^2\right) \prod_{a,\mu} \delta\left(\epsilon_{\mu\nu\lambda}\Delta_\nu F_{a\lambda} - 2S\eta_i\delta_{\mu\tau}\right) \tag{2.5}$$

Here the sum is over the integer-valued field $F_{a\mu}$ which resides on the sites of the dual cubic lattice in spacetime; the delta function constraint imposes 'Gauss's law' (2.1) and the 'Maxwell equation' between E and B which follows from the matrix elements of (2.4). The time spacing $\Delta\tau$ has been chosen so that the coupling $e^2 = K_1\Delta\tau = 1/(K_2\Delta\tau)$.

We now solve the constraint in (2.5) by writing $F_{a\mu}$ as the sum of a particular solution and the general solution of the homogeneous equation:

$$F_{a\mu} = \Delta_\mu N_a + 2S\mathcal{X}_{a\mu}. \tag{2.6}$$

Here N_a is a fluctuating integer-valued field on the dual lattice sites, while $\mathcal{X}_{a\mu}$ is a *fixed* field independent of τ satisfying

$$\epsilon_{\mu\nu\lambda}\Delta_\nu\mathcal{X}_{a\lambda} = \eta_i\delta_{\mu\tau}. \tag{2.7}$$

A convenient choice is to take $\mathcal{X}_{ax} = 0$, $\mathcal{X}_{a\tau} = 0$, and $\mathcal{X}_{ay}$ as shown in Fig 2a, taking the values ± 1 on every second column of sites and zero otherwise. For future manipulations, it is convenient to split $\mathcal{X}_{a\mu}$ into curl-free and divergence-free parts by writing

$$\mathcal{X}_{a\mu} = \Delta_\mu\mathcal{Y}_a + \epsilon_{\mu\nu\lambda}\Delta_\nu\mathcal{Z}_{i\lambda}, \tag{2.8}$$

where again $\mathcal{Y}_a$ and $\mathcal{Z}_{i\mu}$ are fixed fields independent of τ and their values are shown in Fig 2b,c; $\mathcal{Y}_a$ takes the values $0, 1/4, 1/2, 3/4$ on the four dual sublattices, while $\mathcal{Z}_{i\mu} = \delta_{\mu\tau}\eta_i/8$.

We have now assembled all the ingredients necessary for the final representations of the partition function. There are three different formulations, and each present a valuable physical perspective and can be used for further quantitative analysis. We will present them in turn in the following subsections.

1. *Height model*

We insert (2.6) into (2.5) and obtain the height model partition function

$$Z_H = \sum_{\{N_a\}} \exp\left(-\frac{e^2}{2}\sum_{a,\mu}\left(\Delta_\mu N_a + 2S\mathcal{X}_{a\mu}\right)^2\right). \tag{2.9}$$

For the purposes of this section, it is convenient to insert the decomposition (2.8) in (2.9) and obtain[4, 5, 13]

$$Z'_H = \sum_{\{N_a\}} \exp\left(-\frac{e^2}{2}\sum_{a,\mu}\left(\Delta_\mu H_a\right)^2\right), \tag{2.10}$$

where the 'heights' H_a are defined by

$$H_a = N_a + 2S\mathcal{Y}_a. \tag{2.11}$$

Notice that $\mathcal{Z}_a$ has dropped out–this is a general property of all representations of bipartite dimer models, but the non-bipartite models in Section II B will depend upon $\mathcal{Z}_a$. We can view H_a as the heights of a 3-dimensional interface which are restricted to take values equal (for $S = 1/2$) to those in Fig 2b plus arbitrary integers. It is instructive to note here, for $S = 1/2$, a direct connection between these heights and the original dimer model we began with[18]. For large e^2, the partition function Z'_H will be dominated by configurations in which neighboring heights are as close to each other as possible; the manifold of minimum action is defined by heights which satisfy

$$|H_a - H_b| < 1 \ \text{ for every pair of nearest neighbors } a, b, \tag{2.12}$$

If we consider two height configurations to be equivalent if they differ only by a constant integer shift $H_a \to H_a + p$, then the set of all such equivalence classes is precisely equivalent to the set of dimer coverings. The identification is illustrated in Fig 3: neighboring heights differ either by large (3/4) or small (1/4) steps, and we place a dimer on every link intersecting a large step.

2. *sine-Gordon model*

Promote the integer valued field N_a to a real-valued field φ_a by the Poisson summation formula. After shifting the real field by $\varphi_a \to \varphi_a - \mathcal{Y}_a$ we obtain from (2.5,2.6,2.8)

$$Z_{sG} = \prod_a \int_{-\infty}^{\infty} d\varphi_a \sum_{\{P_a\}} \exp\left(-\frac{e^2}{2}\sum_{a,\mu}\left(\Delta_\mu\varphi_a\right)^2 + 2\pi i\sum_a P_a\left(\varphi_a - \mathcal{Y}_a\right)\right). \tag{2.13}$$

If we now truncate the summation over P_a by adding a fugacity $e^{(\ln y)P_a^2}$, then $\sum_{p_a} e^{2\pi i P_a(\varphi_a - \mathcal{Y}_a) + (\ln y)P_a^2} \approx e^{2y\cos(2\pi(\varphi_a - \mathcal{Y}_a))}$, and Z_{sG} is seen to be a version of the sine-Gordon field theory in 2+1 dimensions[4, 5].

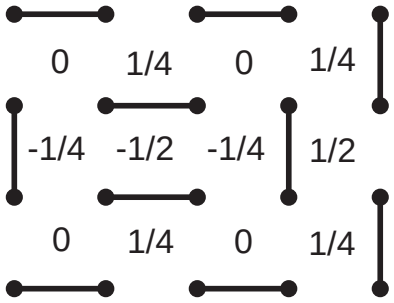

FIG. 3: A set of values of H_a satisfying (2.12) and the corresponding dimer covering.

3. Compact QED

Define $M_{a\mu} = \Delta_\mu N_a$; so $M_{a\mu}$ is an integer-valued field satisfying the constraints

$$\epsilon_{\mu\nu\lambda}\Delta_\nu M_{a\lambda} = 0. \tag{2.14}$$

We impose these constraints by a real Lagrange multiplier field $A_{i\mu}$ by inserting factors of

$$\int_{-\pi}^{\pi} \frac{dA_{i\mu}}{2\pi} \exp\left(iA_{i\mu}\epsilon_{\mu\nu\lambda}\Delta_\nu M_{a\lambda}\right) \tag{2.15}$$

in Z_H in (2.9). The sum over the $M_{a\mu}$ can now be performed using the Poisson summation formula and we obtain after using (2.7)

$$Z_{cQED} = \sum_{\{Q_{a\mu}\}} \prod_{i,\mu} \int_{-\pi}^{\pi} \frac{dA_{i\mu}}{2\pi} \exp\left(-\frac{1}{2e^2}\sum_{i,\mu}\left(\epsilon_{\mu\nu\lambda}\Delta_\nu A_{i\lambda} - 2\pi Q_{a\mu}\right)^2 + i2S\sum_i \eta_i A_{i\tau}\right), \tag{2.16}$$

where the $Q_{a\mu}$ extend over all integers. Z_{cQED} is easily seen to be the Villain form of the partition function of a compact $U(1)$ gauge theory in 2+1 dimensions. There is an additional Berry phase carried by the world lines of the background charge density of $2S$ particles on each site. An alternative, and exactly equivalent, form of Z_{cQED} can be obtained by applying the above transformation to Z'_H (in (2.10)) rather than to Z_H. Then, exactly the same steps lead to

$$Z'_{cQED} = \sum_{\{Q_{a\mu}\}} \prod_{i,\mu} \int_{-\pi}^{\pi} \frac{dA_{i\mu}}{2\pi} \exp\left(-\frac{1}{2e^2}\sum_{i}\left(\epsilon_{\mu\nu\lambda}\Delta_\nu A_{i\lambda} - 2\pi Q_{a\mu}\right)^2 + i4\pi S\sum_a \mathcal{Y}_a \Delta_\mu Q_{a\mu}\right) \tag{2.17}$$

The instanton number of the gauge theory is $\Delta_\mu Q_{a\mu}$, and to the Berry phase is now carried by the instantons: each instanton has a Berry phase of $e^{i4\pi S\mathcal{Y}_a}$. It is a remarkable fact that precisely the *same Berry phase* was obtained in very different semiclassical and large N analysis of bipartite antiferromagnets[5, 19]. It is also worth reiterating that Z_{cQED} (in which the Berry phase is carried by the world lines of the $2S$ particles on each site) and Z'_{cQED} (in which the Berry phase is associated with the instantons) are exactly equivalent[13]—they merely do the book-keeping of the total Berry phase somewhat differently.

The properties of the theories Z'_H, Z_{sG}, and Z'_{cQED} are reasonably well understood and have been described elsewhere[5, 13, 18]. The height model is in a smooth phase phase for

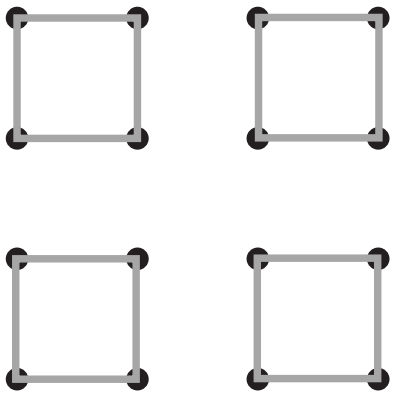

FIG. 4: Another possible ground state of the dimer model: the plaquette state.

all values of e^2 (there is no roughening transition), while the compact $U(1)$ gauge theory is always confining. In terms of the underlying dimer model, this means that translational symmetry is spontaneously broken and the dimers crystallize in a bond-charge ordered state. A likely configuration is the columnar state in Fig 1a, but it is not ruled out that one of these theories could exhibit a transition to some other confining state in which the details of the lattice symmetry breaking are different: another state[20] which occurs in the parameter space of Z_{sG} is the plaquette state of Fig 4.

B. Non-bipartite dimer models

We will now relax the constraint that the dimers must connect sites on opposite sublattices. We will show that such a step reduces the height model to a 2+1 dimensional fully frustrated Ising model in a transverse field, following the derivation[15] outlined in Ref[14].

An example of a dimer state connecting sites on the same sublattice is shown in Fig 5a. Notice that a pair of such 'diagonal' dimers can resonate with a pair of dimers connecting opposite sublattices. However models which include terms like those in Fig 5a do not appear to be amenable to the *exact* duality transformations we have considered in Section II A. So we have two alternatives for further analysis: we could be satisfied by approximate duality transformations on models which include the resonance in Fig 5a, or we could modify the underlying dimer model to allow duality to proceed smoothly. Both alternatives lead to essentially the same final result, but we will choose the latter for presentation here as it more clearly isolates the approximation made. The modification of the dimer model is aided by the physical picture developed in the large-N theories of the effects of frustration presented in Refs [21, 22]. The key property of the diagonal dimers in Fig 5a is that they connect sites on the same sublattice, and such dimers carry net charge ± 2 under the compact QED representation of Section II A 3. This will be shown explicitly in more detail below, but can be seen quickly as follows. From the representation (2.16) we see that the model behaves as if there are background charges of $+2S$ on one sublattice, and charges of $-2S$ on the other sublattice. A dimer connecting sites on opposite sublattices absorbs (in the Gauss Law constraint (2.1)) charges of ± 1 on its two ends; so such a dimer has net charge 0. However we do need a vector potential for a gauge invariant connection between the charges on the two ends, and this is why the number operator of the dimer $\sim e^{iA_{i\alpha}}$ (see

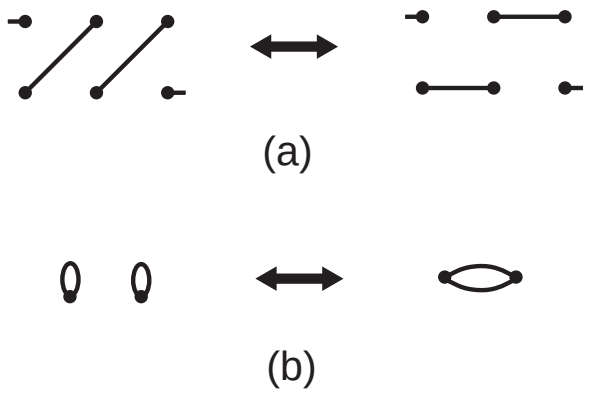

FIG. 5: (a) Dimers which connect sites on the same sublattice resonating with dimers connecting sites on opposite sublattices. (b) The same sublattice dimers have now been collapsed onto monomers representing singlet bonds between electrons on the same site. We argue that the deformation from (a) to (b) should have no significant effect on the long distance properties: it is crucial to keep track of which sublattice the two ends of a singlet bond reside, and local deformations which preserve this information will not modify the long distance physics. The diagonal dimers in (a) and the monomers in (b) both carry net charge ± 2, and this is the key factor which controls their effect on the long distance physics.

(2.2)). Let us now apply the same argument to the diagonal dimers of Fig5a. These connect sites on the same sublattice and therefore carry net charge ± 2; however, we also need a vector potential to connect such spatially separated charges, and so the number operator of a diagonal operator must also contain the necessary path integral of $A_{i\alpha}$. It is this combined role of diagonal dimers that precludes a straightforward duality transformation, but it also suggests a simplifying modification: the important thing is that the dimer carry charge ± 2 while preserving the fact that each site has net charge $\pm 2S$; so we collapse the two ends of the diagonal dimers onto the same site, as in Fig 5b. The resulting *monomer* trivially satisfies the requirement of representing a singlet bond between electrons on the same sublattice and thus carries charge ± 2; moreover, no vector potential is required as the charges on its two ends are on the same spatial location. Further, such monomers can resonate, like the diagonal dimers, between dimers connecting sites on opposite sublattices, as shown in Fig 5. Of course such a model requires that the number of singlet bonds allowed to emerge from a site be at least two *i.e.* $2S \geq 2$. Nevertheless, we maintain that generic properties of the model studied here apply also to $S = 1/2$ models with configurations such as those in Fig 5a.

Let us now write down the Hamiltonian of the monomer-dimer model containing the resonance in Fig 5b. Let $\eta_i \hat{n}_i$ be the monomer number operator on site i. Then the constraint that there are exactly $2S$ singlet bonds emerging from site i modifies the 'Gauss Law' constraint (2.1) to

$$\Delta_\alpha \hat{E}_{i\alpha} + 2\hat{n}_i = 2S\eta_i. \tag{2.18}$$

This equation shows that in addition to the background 'charge' of $2S$, there is[21, 22], as claimed above, a fluctuating charge density of a 'Higgs field' of monomers of charge 2. We

also introduce a angular phase variable $\hat{\phi}_i$ canonically conjugate to $\hat{n}_i$:

$$[\hat{\phi}_i, \hat{n}_j] = i\delta_{ij} \tag{2.19}$$

We can easily now extend the dimer Hamiltonian H_d in (2.3) to include the resonance in Fig 5b, induced by the following cosine term proportional to K_4:

$$\widetilde{H}_d = \frac{K_1}{2}\sum_{i,\alpha}\hat{E}_{i\alpha}^2 + \frac{K_3}{2}\sum_i \hat{n}_i^2 - K_2\sum_i \cos(\epsilon_{\alpha\beta}\Delta_\alpha \hat{A}_{i\beta}) - K_4\sum_{i,\alpha}\cos(\Delta_\alpha\hat{\phi}_i - 2\hat{A}_{i\alpha}). \tag{2.20}$$

For convenience we have also added an additional term, proportional to K_3, which controls the density of monomer fluctuations.

The remainder of this subsection describes the analysis of the Hamiltonian $\widetilde{H}_d$, with the quantum dynamics defined by the commutation relations (2.2) and (2.19), while preserving the local constraint (2.18). The procedure will closely parallel that followed in Section II A. We insert complete sets of $\hat{E}_{i\alpha}$ and $\hat{n}_i$ eigenstates at intervals of imaginary time $\Delta\tau$ in the partition function. As in (2.4), we replace the exponential of the new cosine term proportional to K_4 by a Villain form but with a decoupling field $k_{i\alpha}$. After evaluating the matrix elements between the complete sets of states, defining the three-vector integer-valued 'current' $j_{i\mu} = (k_{ix}, k_{iy}, -n_i)$ we find that Z_F in (2.5) is replaced by

$$\widetilde{Z}_F = \sum_{\{F_{a\mu}\},\{j_{i\mu}\}} \exp\left(-\frac{e^2}{2}\sum_{a,\mu}F_{a\mu}^2 - \frac{g}{2}\sum_{i,\mu}j_{i\mu}^2\right)\prod_{a,\mu}\delta\left(\epsilon_{\mu\nu\lambda}\Delta_\nu F_{a\lambda} + 2j_{i\mu} - 2S\eta_i\delta_{\mu\tau}\right)\prod_i \delta(\Delta_\mu j_{i\mu}), \tag{2.21}$$

where, for simplicity, we have chosen the coupling $g = K_3\Delta\tau = 1/(K_4\Delta\tau)$. The sum in (2.21) is over integer valued fields $F_{a\mu}$, on the dual lattice, and $j_{i\mu}$ on the direct lattice. The solution of the constraints analogous to (2.6) is

$$\begin{aligned} j_{i\mu} &= \epsilon_{\mu\nu\lambda}\Delta_\nu a_{a\lambda} \\ F_{a\mu} &= \Delta_\mu N_a - 2a_{a\mu} + 2S\mathcal{X}_{a\mu}, \end{aligned} \tag{2.22}$$

where $a_{a\mu}$ is an integer-valued 'gauge' field on the links of the dual lattice, while, as before, N_a is an integer-valued height field on the sites of the dual lattice. Inserting (2.22) into (2.21) we obtain the generalization of the height model (2.9)

$$\widetilde{Z}_H = \sum_{\{N_a\},\{a_{a\mu}\}} \exp\left(-\frac{e^2}{2}\sum_{a,\mu}\left(\Delta_\mu N_a - 2a_{a\mu} + 2S\mathcal{X}_{a\mu}\right)^2 - \frac{g}{2}\sum_{a,\mu}\left(\epsilon_{\mu\nu\lambda}\Delta_\nu a_{a\lambda}\right)^2\right). \tag{2.23}$$

We will refer to this partition function as the 'gauged height model'; the form (2.23) is the most convenient for subsequent analysis and is one of the key expressions of this paper. We also note an alternative form of $\widetilde{Z}_H$, analogous to (2.10), obtained by inserting (2.8) into (2.23)

$$\widetilde{Z}'_H = \sum_{\{N_a\},\{a_{a\mu}\}} \exp\left(-\frac{e^2}{2}\sum_{a,\mu}\left(\Delta_\mu H_a - 2a_{a\mu}\right)^2 - \frac{g}{2}\sum_{a,\mu}\left(\epsilon_{\mu\nu\lambda}\Delta_\nu a_{a\lambda} - \frac{2Se^2}{g}\mathcal{Z}_{i\mu}\right)^2\right), \tag{2.24}$$

where the heights H_a are defined in (2.11). As promised earlier, $\mathcal{Z}_{i\mu}$ does not drop out of the models of this subsection.

The main remaining task is to describe the physical properties of the gauged height model (2.23); we will embark on this in Section II B 2. However, before we do so, we will, for completeness, present the analog of the compact QED models of Section II A 3.

1. Compact QED

We apply the method of Section II A 3 to $\widetilde{Z}_H$. We define integer-valued fields $M_{a\mu} = \Delta_\mu N_a - 2a_{a\mu}$ and $b_{i\mu} = \epsilon_{\mu\nu\lambda}\Delta_\nu a_{a\lambda}$ which satisfy the constraints $\epsilon_{\mu\nu\lambda}\Delta_\nu M_{a\lambda} + 2b_{i\mu} = 0$ and $\Delta_\mu b_{i\mu} = 0$. Imposing these constraints by continuous real fields $A_{i\mu}$ and ϕ_i respectively, and performing the summation over $M_{a\mu}$ and $b_{i\mu}$ by the Poisson summation formula we obtain

$$\widetilde{Z}_{cQED} = \sum_{\{Q_{a\mu}\},\{p_{i\mu}\}} \prod_{i,\mu} \int_{-\pi}^{\pi} \frac{dA_{i\mu}}{2\pi} \prod_i \int_{-\pi}^{\pi} \frac{d\phi_i}{2\pi} \exp\left(-\frac{1}{2e^2} \sum_{i,\mu} (\epsilon_{\mu\nu\lambda}\Delta_\nu A_{i\lambda} - 2\pi Q_{a\mu})^2 - \frac{1}{2g} \sum_{i,\mu} (\Delta_\mu \phi_{i\mu} - 2A_{i\mu} - 2\pi p_{i\mu})^2 + i2S \sum_i \eta_i A_{i\tau} \right), \quad (2.25)$$

where $Q_{a\mu}$ and $p_{i\mu}$ extend over all the integers. This is the Villain form of the action of compact QED coupled to a charge 2 Higgs scalar[4, 22]. The Berry phase term, attributable to the background charge density of $2S\eta_i$ on each site, is the same as that in Z_{cQED} in (2.16). If, as in Section II A 3, we had applied the transformation of this subsection to $\widetilde{Z}'_H$ rather than $\widetilde{Z}_H$, then the Berry phases would have been attached to the monopoles and vortices of the compact QED theory[14]; this is straightforward to do and we will not explicitly present the results here—the final form is, of course, exactly equivalent to (2.25), (2.24) or (2.23). Also note that the $g = \infty$ limit of $\widetilde{Z}_{cQED}$ in (2.25) is exactly equal to Z_{cQED} in (2.16).

2. Gauged height models

We now return to the main objective of this section: determination of the phase diagram of the gauged height model $\widetilde{Z}_H$ in (2.23). We will restrict our attention to $S = 1/2$; results for other half-odd-integer values of S are similar, and the generalization to integer S is straightforward.

As in the work by Fradkin and Shenker [23], it is useful to look at various limiting values of the couplings in $\widetilde{Z}_H$: from these results we have constructed the phase diagram shown in Fig 6.

(i) $g = \infty$:

The field $a_{a\mu}$ must be 'pure gauge' along this line, with $a_{a\mu} = \Delta_\mu c_a$ for some integer-valued c_a. This can be absorbed in N_a by $N_a \to N_a + 2c_a$, and so $\widetilde{Z}_H$ reduces to the pure height model Z_H considered in (2.9) in Section II A. So the heights are in a smooth phase, the gauge theory is confining, and there is translational symmetry breaking due to the presence of bond-charge-density order.

(ii) $e^2 = 0$:

Now the height field N_a drops out, and the theory is simply that of the integer-valued gauge field $a_{a\mu}$ with a Maxwell action. This theory is exactly equivalent to the pure XY model in 2+1 dimensions, as can be seen by setting $A_{i\mu} = Q_{a\mu} = 0$ in (2.25). So there is a phase transition in the D=3 XY universality class at a critical $g = g_c$; the $g < g_c$ ($g > g_c$) phase maps onto the low (high) temperature phase of the XY model.

(iii) $g = 0$:

This is the most interesting limit, where new physics emerges. With no Maxwell term for the gauge field $a_{a\mu}$, the sum over $a_{a\mu}$ can be performed independently on each link. From

this it is evident that only the *parity* of the N_a is relevant–the partition function depends only upon whether a given N_a is even or odd. So we can introduce an Ising spin variable, σ_a on each site of the dual lattice by defining

$$\sigma_a = 2\left[N_a (\mathrm{mod}\ 2)\right] - 1. \tag{2.26}$$

In terms of the σ_a, $\widetilde{Z}_H$ reduces to the Ising partition function in three dimensions[14]

$$Z_I = \sum_{\{\sigma_a = \pm 1\}} \exp\left(- \sum_{<a,b>} J_{ab}\sigma_a\sigma_b \right). \tag{2.27}$$

The sum a, b is over nearest neighbor pairs on the dual cubic lattice. The exchange constants J_{ab} all satisfy $|J_{ab}| = J(e^2)$ where $J(e^2)$ is a monotonically increasing function defined by

$$e^{2J(e^2)} \equiv \left[\sum_{n=-\infty}^{\infty} e^{-2n^2e^2} \right] / \left[\sum_{n=-\infty}^{\infty} e^{-(2n+1)^2e^2/2} \right]. \tag{2.28}$$

The presence of the $\mathcal{X}_{a\mu}$ in $\widetilde{Z}_H$ introduces a key variation in the signs of the J_{ab}: it is not difficult to see that these signs must be chosen so that each plaquette in the x-y plane is frustrated[14]. In the language of 2+1 dimensional quantum models, this is the fully frustrated Ising model in a transverse field[24]. Such a model has been studied in earlier works [14, 25, 26], and we summarize the main results. There is a phase transition at [14, 26] $e^2 = e_c^2$ where $J(e_c^2) \approx 0.35$, such that for $e^2 > e_c^2$ both the Ising symmetry ($\langle\sigma_a\rangle \neq 0$) and the translational symmetry are simultaneously broken. The broken translational symmetry is due to development of columnar spin Peierls order of the type shown in Fig 1a. In the language of the gauge theory, $\widetilde{Z}_{cQED}$, this phase is confining. For $e^2 < e_c^2$, the gauge theory is in the deconfined 'Higgs' phase, and Ising and translational symmetries are restored. This mechanism of deconfinement of spinons in antiferromagnets by condensation of a charge 2 Higgs field was first proposed in Ref [21]. The condensation of the Higgs field means that there are strong fluctuations in the conjugate number operator *i.e.* in the number of dimers carrying charges ± 2—these can fluctuate into dimers of net charge 0, without violating the number constraint which fixes the total number of singlet bonds from each site at $\pm 2S$, as shown in Fig 5. According to the arguments of Refs [14, 25] the phase transition in the fully frustrated Ising model at $e^2 = e_c^2$ is also in the XY universality class, but now the $e^2 > e_c^2$ ($e^2 < e_c^2$) region maps onto the low (high) temperature phase of the XY model. Finally we note that the simulations of Grest [26] appear to observe a second phase transition at $e^2 = e_{2c}^2$ where $J(e_{2c}^2) \approx 1.8$: for $e^2 > e_{2c}^2$ the pattern of the translational symmetry breaking appears to change into the plaquette phase of Fig 4—however the gauge theory remains in the confining phase.

(*iv*) $e^2 = \infty$:

The physics here is very similar to the large e^2 region considered in (*iii*) at $g = 0$—translational and Ising symmetries are broken and the gauge theory is confining.

All of the above results have been combined in Fig 6 which is one of the central results of this paper. There is a single phase boundary connecting the phase transitions at $e^2 = 0$, $g = g_c$ and $e^2 = e_c^2$, $g = 0$ found above. By familiar arguments [23] it is expected that the universality class of the transition along this entire line will be the same as that of the $e^2 = e_c^2$, $g = 0$ point, and the $e^2 = 0$, $g = g_c$ point is a singular limit.

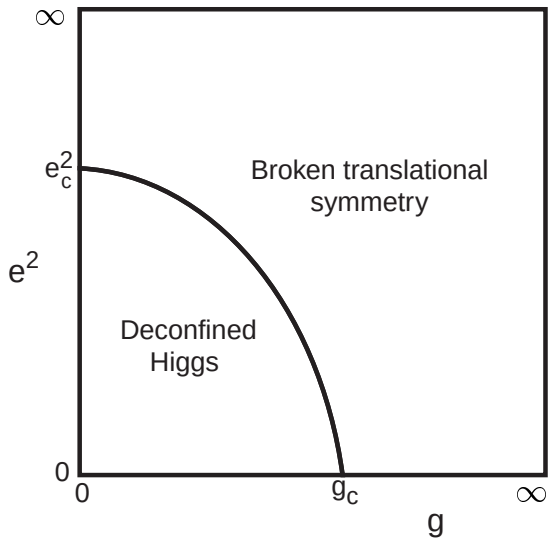

FIG. 6: Phase diagram of the gauged height model $\widetilde{Z}_H$ in (2.23) for $S = 1/2$; the same phase diagram also applies to the height model $\widetilde{Z}'_H$ in (2.24), or to the exactly equivalent compact QED + charge 2 Higgs scalar theory $\widetilde{Z}_{cQED}$ in (2.25). There is no translational symmetry breaking in the 'deconfined Higgs' phase. The phase with translational symmetry breaking is confining; however, it is not completely ruled out that a portion of it could be deconfining, although no such deconfined phase with broken translational symmetry appears in Refs [14, 25, 26]. Most of the translational symmetry breaking is in the columnar pattern of Fig 1a; however for very large e^2 there appears to be [26] a change by a first order transition into the plaquette state of Fig 4–this is not shown. The entire phase transition line bounding the deconfined, Higgs phase (apart from the single point $e^2 = 0$, $g = g_c$) is described by the fully-frustrated Ising model in a transverse field, Z_I in (2.27): this transition is expected to be in the $D = 3$ XY universality class, with the *high* temperature phase of the XY model corresponding to the Higgs phase. The transition at $e^2 = 0$, $g = g_c$ is also in the $D = 3$ XY universality class, but it is inverted with respect to the previous one—now the *low* temperature phase of the XY model is the Higgs phase.

III. DOPED ANTIFERROMAGNETS

We now discuss recent work[8] which examined the consequences of hole-doping the state with broken translational symmetry in Fig 6. A theory for hole-doping the deconfined Higgs phase of Fig 6 does not exist and would be an interesting direction for future work.

The study was carried out in a particular large N limit in which the columnar spin-Peierls state of Fig 1a was a ground state in mean-field theory. Further, the ordering in the state was fully developed, and the ground state was well separated from any possible phase transition to a deconfined Higgs phase or to a magnetically ordered state. This is probably not a realistic situation for the insulator, but it is expected that the results so obtained are generic for doping an arbitrary spin-Peierls phase. The results of the study have also been reviewed recently[9], and so we will limit ourselves here to highlighting the main results and mentioning some experimental implications.

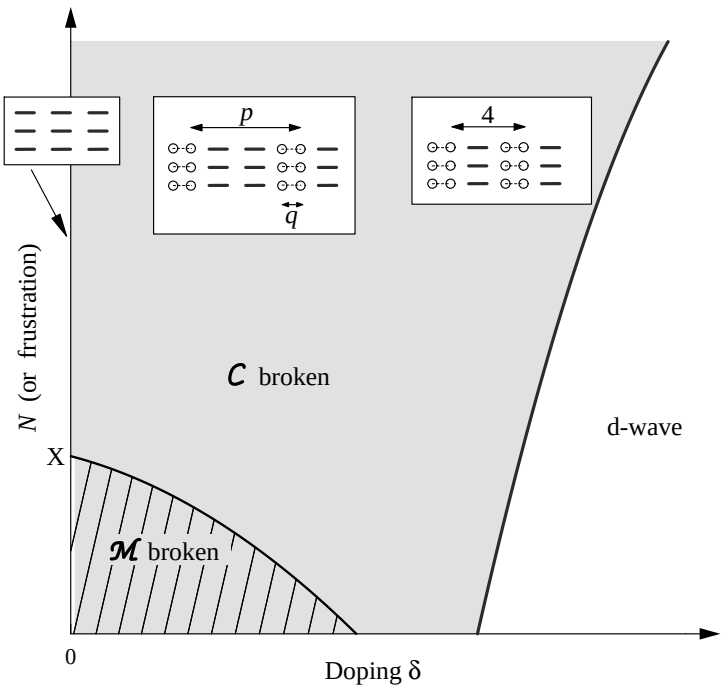

FIG. 7: Ground state phase diagram of a doped antiferromagnet, adapted from Ref [8]. $\mathcal{M}$ is the symmetry of spin rotations and it is broken in the hatched region, while $\mathcal{C}$ is the translational symmetry which broken in the shaded region. At zero doping, the physical system has Néel order and so $\mathcal{M}$ is broken. By using some frustration in the spin Hamiltonian (or considering models with a larger spin symmetry group (large N)), we move the system across the quantum critical point X into state with columnar spin-Peierls (bond-charge-density) order. The states obtained by doping this state are sketched: the thick and dashed lines indicate varying values of the bond charge density, while the circles represent site hole density. All the states with non-zero hole density are superconducting for large enough N, but could undergo phase transitions to insulating, anisotropic Wigner crystalline states as N is reduced.

As in Refs [6, 7], the main effect found was that for reasonable values of the microscopic parameters, the holes prefer to segregate in one-dimensional striped structures with a finite density per unit length—so as the net hole concentration tends to zero, the stripes move farther apart but maintain a finite hole density per unit length per stripe. However, the existence of a background of spin-Peierls order makes the details of the hole configurations quite different from earlier work [6, 7, 27] in experimentally significant ways, as we detail below. A schematic for the evolution of the hole configuration is indicated in the phase diagram in Fig 7.

The unit cells of the charge ordered states in Fig 7 have size $p \times 1$; within each unit cell, the holes are concentrated in a region of size $q \times 1$. Both p and q were always found to be even, with q remaining fixed while $p \to \infty$ as the doping concentration $\delta \to 0$. Significant properties of these even-width stripes are:

- The holes density per unit length in the q-width region is not unity (as found in earlier theories [6, 7]) but various continuously dependent upon microscopic parameters. For reasonable choices we can obtain a hole density per unit length of around 0.5 (for $q = 2$

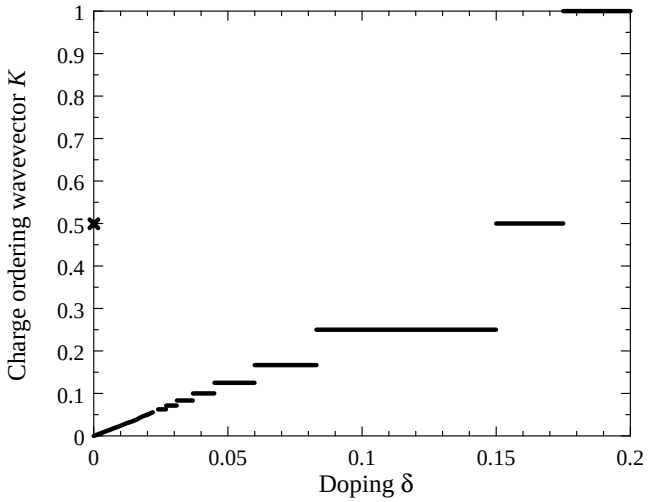

FIG. 8: Charge ordering wavevector $(1/p)$ as a function of the doping, δ (from Ref [8]).

this corresponds to a ladder with $\approx 1/4$ hole per site), but it is never pinned at exactly this value for any finite range of doping, δ *i.e.* the stripes are not incompressible.

- There are strong pairing correlations between the holes in each q-width region. This leads to an anisotropic superconducting ground state, and should allow good metallic conduction above the superconducting transition temperature. These characteristics are consistent with observations[28] on $La_{2-x-y}Nd_ySr_xCuO_4$.

- The evolution of the charge ordering wavevector ($K = 1/p$) as a function of doping, δ, is shown in Fig 8. Note that this wavevector is always quantized at values which equal 1/(even integer). The plateaus are quite small for small δ, but become progressively broader as the even integer decreases. In particular, as is observed experimentally, a large plateau at wavevector 1/4 is present and this emerges naturally from our theory–we regard this as significant. Plateaus at smaller wavevector (say 1/6) have not been experimentally observed, but the resolution of current experiments is not precise enough to distinguish the staircase-like evolution in Fig 8 from a continuous variation before reaching the plateau at 1/4. The hole density per unit length of stripe varies continuously within each plateau but jumps discontinuously as the transition is made from one plateau to the next.

- Note that, in Fig 8, before reaching the d-wave superconducting state with $p = 1$, there is also a small plateau at $p = 2$: this is a state with uniform site-charge density, but with the bond-charge density of Fig 1a coexisting with d-wave-like superconductivity. Such a state has not been observed, and it would be interesting to look for one.

- All of the stripes found in this computations are bond-centered, at least in the region where the symmetry of spin-rotations, $\mathcal{M}$, remains unbroken; we cannot rule out the possibility that there will be a transition to site-centered stripes, like those found earlier [6, 7], once $\mathcal{M}$ is broken. It would be useful for future experiments to detect this distinction between bond-centered and site-centered stripes. Let us discuss this difference more precisely for the case $p = 4$. For the site-centered stripe, the hole density per unit length in each column of sites takes values ρ_1, ρ_2, ρ_3, ρ_2

before repeating periodically (where ρ_{1-3} are some three distinct densities); this is the configuration usually assumed in most experimental papers. In contrast for the bond-centered state, these densities take the values ρ_1, ρ_1, ρ_2, ρ_2, and this also appears to be compatible with existing observations. In the computation here the bond-centering is important for enhancing pairing correlations, which are responsible for superconducting/metallic transport in the direction parallel to the stripes. We note that a very recent NQR experiment[29] indicates a charge distribution which has some features consistent with the bond-centered state: they find only two inequivalent sites associated with the stripes, and a density per site in the hole-rich region which is only about 0.18-0.19 (the fully segregated site-centered stripe would have $\rho_1 \approx 0.5$, $\rho_2 = \rho_3 = 0$, while the fully segregated bond-centered stripe would have $\rho_1 \approx 0.25$, $\rho_2 = 0$; clearly the bond-centered value is more compatible with observations).

Acknowledgements

We thank G. Teitel'baum, S. Uchida, Jan Zaanen, and especially Matthew Fisher and T. Senthil for useful discussions. We are particularly grateful to the last two for describing their results prior to publication. S.S. thanks Masashi Takigawa for organizing a stimulating conference, and wishes Prof. Yasuoka many more productive years. This research was supported by US NSF Grant No DMR 96–23181 and by the DFG (VO 794/1-1).

---

[1] J. M. Tranquada, J. Phys. Chem. Solids **59**, 2150 (1998).
[2] S. Wakimoto *et al*, Phys. Rev. B **60**, R769 (1999); Y. S. Lee *et al*, *ibid* **60**, 3643 (1999).
[3] A. W. Hunt, P. M. Singer, K. R. Thurber, and T. Imai, Phys. Rev. Lett. **82**, 4300 (1999); T. Imai, C. P. Slichter, K. Yoshimura, and K. Kosuge, Phys. Rev. Lett. **70**, 1002 (1993); T. Imai, C. P. Slichter, K. Yoshimura, M. Katoh, and K. Kosuge, Phys. Rev. Lett. **71**, 1254 (1993); S. Fujiyama M. Takigawa, Y. Ueda, T. Suzuki, and N. Yamada, cond-mat/9904275.
[4] N. Read and S. Sachdev, Phys. Rev. Lett. **62**, 1694 (1989).
[5] N. Read and S. Sachdev, Phys. Rev. B **42**, 4568 (1990).
[6] J. Zaanen and O. Gunnarsson, Phys. Rev. B **40**, 7391 (1989).
[7] H. Schulz, J. de Physique **50**, 2833 (1989).
[8] M. Vojta and S. Sachdev, Phys. Rev. Lett. **83**, Nov 8 (1999); cond-mat/9906104.
[9] S. Sachdev and M. Vojta, cond-mat/9908008.
[10] D. Rokhsar and S. A. Kivelson, Phys. Rev. Lett. **61**, 2376 (1988).
[11] N. Read and S. Sachdev, Nucl. Phys. B **316**, 609 (1989).
[12] E. Fradkin and S. Kivelson, Mod. Phys. Lett. B **4**, 225 (1990).
[13] R. A. Jalabert and S. Sachdev, Mod. Phys. Lett. B **4**, 1043 (1990).
[14] R. A. Jalabert and S. Sachdev, Phys. Rev. B **44**, 686 (1991).
[15] S. Sachdev, unpublished notes, July 30, 1990, available at http://onsager.physics.yale.edu/qdnotes.pdf
[16] T. Senthil and M. P. A. Fisher, cond-mat/9910224.
[17] N. Nagaosa and P. A. Lee, cond-mat/9907019.
[18] W. Zheng and S. Sachdev, Phys. Rev. B **40**, 2704 (1989).
[19] F. D. M. Haldane, Phys. Rev. Lett. **61**, 1029 (1988).

[20] S. Sachdev and N. Read, Phys. Rev. Lett. **77**, 4800 (1996), footnote 19.
[21] N. Read and S. Sachdev, Phys. Rev. Lett. **66**, 1773 (1991).
[22] S. Sachdev and N. Read, Int. J. Mod. Phys. B **5**, 219 (1991).
[23] E. Fradkin and S. H. Shenker, Phys. Rev. D **19**, 3682 (1979).
[24] It is also instructive to take the $g = 0$ limit of the action, $\widetilde{Z}_{cQED}$, for compact QED coupled to a charge 2 Higgs scalar in (2.25). Then in a suitable gauge $A_{i\mu}$ is pinned to 0 or π. We can now define an Ising *gauge* field $\zeta_{i\mu} = e^{iA_{i\mu}}$, and the action in (2.25) reduces to the standard plaquette action for a 2+1 dimensional Z_2 gauge theory on the direct lattice. The Berry phase term contributes a factor $\prod_i \zeta_{i\tau}^{2S}$ to the partition function, and this is the representation of the frustration in the dual lattice Ising model Z_I in (2.27).
[25] D. Blankschtein, M. Ma, and A. N. Berker, Phys. Rev. B **30**, 1362 (1984).
[26] G. S. Grest, J. Phys. C: Solid State Phys. **18**, 6239 (1985).
[27] V. J. Emery, S. A. Kivelson, and H. Q. Lin, Phys. Rev. Lett. **64**, 475 (1990); S. A. Kivelson, V. J. Emery, and H. Q. Lin, Phys. Rev. B **42**, 6523 (1990).
[28] N. Ichikawa, S. Uchida, J. M. Tranquada, T. Niemoeller, P. M. Gehring, S.-H. Lee, and J. R. Schneider, cond-mat/9910037.
[29] G. B. Teitel'baum, B. Büchner, and H. de Gronckel, cond-mat/9910036.